

Comparative Study of Concrete Constitutive Models for Predicting Blast Response

James W. Wesevich, David D. Bogosian, Barry L. Bingham,
Johan Magnusson, and Alexander P. Christiansen

Baker Engineering and Risk Consultants

3330 Oakwell Court, Suite 100, San Antonio, TX 78218-3024

E-mail: JWesevich@BakerRisk.com

Synopsis: The robustness of concrete constitutive material models in explicit finite element codes is typically measured by their ability to match peak dynamic and permanent displacements of a reinforced concrete specimen. In a series of recent shock tube experiments, reinforced concrete slabs were subjected to simulated blast loads. Applied pressure histories were recorded in these tests, as were peak and residual displacements. This paper evaluates the Concrete Damage Model (Material 72, Release 3) and the Continuous Surface Cap Model (Material 159) within LS-DYNA (Version 971), as well as the Applied Engineering Cap model (AEC-3I) in DYNA3D. The results indicate some variation in predicted damage and failure modes between the three material models, but overall, all three models produced satisfactory comparisons to the test with regard to peak positive deflection (i.e., within a factor of 2 of the measured response). A surprising outcome is that the inclusion of rate-dependent material properties actually increased the error in the predicted response. In terms of predicting crack patterns, the AEC-3I model appears to be preferable, whereas MAT72R3 is preferred for predicting peak deflection. Overall, MAT159 was the most consistent predictor and the least sensitive to variations in the rate dependent properties of concrete.

Keywords: concrete, constitutive, model, blast, deflection, slab, response, shock, tube, test

Author biographical sketches:

James Wesevich, P.E., S.E., is a Senior Principal Engineer and currently manages the Protective Structures Section at BakerRisk. He has spent the last 23 years assessing, designing, and retrofitting buildings under blast loads from vapor cloud, terrorist, conventional weapons, and nuclear explosions. He has also validated structural models with blast testing using DYNA3D and aided in the development and verification of a constitutive material model for concrete. He is a member of ACI Committees 370 and 440-F.

David Bogosian, P.E., has accumulated over 25 years of experience in design and analysis of structures subjected to dynamic and impulsive loading from blast and impact loads. He has been involved in numerous studies in which LS-DYNA was applied to computation of the response of reinforced concrete structures subjected to blast and fragment effects from conventional munitions. He is also a co-author of three chapters in the Design and Analysis of Hardened Structures for Conventional Weapons Effects manual (UFC 3-340-01).

Barry Bingham is a registered Professional Engineer in Colorado and New Mexico with emphasis in structural analysis and design, finite element analysis, coupled thermal/mechanical analysis, Computational Fluid Dynamics (CFD), and engineering model development. Barry has a Bachelor of Science degree from the United States Air Force Academy and a Master of Science from Columbia University. Mr. Bingham authored the AEC-3I model for modeling the behavior of frictional materials (concrete, rock and soils) to very large strains, including failure.

Johan Magnusson obtained an MSc degree in Structural Engineering in 1998. He worked as a Research Engineer for ten years at the Swedish Defense Research Agency conducting research on the effects of weapons on protective structures. Mr. Magnusson joined Baker Engineering and Risk Consultants where he worked for two years as a Senior Engineer. At the end of 2010, he returned to Sweden and commenced his current employment at the Swedish Fortifications Agency.

Alex Christiansen received a B.S. in aerospace engineering and a M.S. in mechanical engineering from the University of California, Los Angeles. His work for both commercial and government clients has focused on the analysis and design of new and existing structures subjected to dynamic and conventional loading. In this work, he has performed many evaluations of structures using high-fidelity finite element models and worked on the development of non-linear material models.

INTRODUCTION

Recent years have seen the increased and widespread use of explicit finite element (FE) models to represent the response of structures to dynamic blast and impact loads. In particular, reinforced concrete structures (typically wall and floor/roof slabs, but also beams, columns, domes, and other geometries) have been the focus of extensive research, using both analytical and experimental techniques. As a result, numerous nonlinear material models have been developed for use in finite element codes to represent concrete response all the way to the most severe damage levels. These models attempt to replicate the complex behaviors of the real material with varying degrees of fidelity, while making available to the analyst a practical means of using FE technology to either predict response or design structural members to resist blast and impact loads.

The purpose of the current paper is to evaluate the ability of three different constitutive concrete models to predict the response of reinforced concrete slabs subjected to blast loads. The models in question are the AEC-3I model (available in DYNA3D), Material 72–Release 3 (available in LS-DYNA), and Material 159 (also in LS-DYNA). The approach taken was to select a set of two well-controlled experiments (one at a moderate level response, the other at a higher level) on a simple one-way reinforced concrete slab and use those results to evaluate all three models. To the extent practicable, other aspects of the modeling process (boundary conditions, blast loads, mesh discretization, representation of rebar) were held constant across all the analyses. The final results are helpful in understanding the sensitivity of calculated response to one's choice of material model. They also indicate each model's ability to replicate various aspects of the experimentally observed response.

The context of the comparisons contained in this paper is that of a consulting engineering practice with a primary focus on computing the response of structures to blast loads from a variety of sources. As such, the material models selected for the comparison are those which are widely used within our company, and to our knowledge, within the broader community of consulting engineers. While perhaps not representative of the latest and technologically most advanced constitutive models (such as those representing crack formation and propagation), they are typical of models used for production calculations supporting building assessments and designs for various real-world applications.

PREVIOUS EXPERIMENTAL RESEARCH

A set of previously performed experiments^[1] was used as a reference for the numerical simulations. The experimental study focused on investigating the blast resistance of reinforced concrete slabs with mechanical reinforcement splices. The slabs were 8.5 ft tall by 8.0 ft wide and 5.5 in thick [2.59 m tall by 2.44 m wide by 140 mm thick]. The concrete was designed to have a nominal 28-day [0.93 month] compressive strength of 4,000 psi [27.6 MPa]. The reinforcement consisted of No. 5 [15.9 mm diameter] steel reinforcing bars spaced at 12 inches [305 mm] on center spanning in the vertical direction and at mid-depth, and with No. 4 bars [12.7 mm diameter] spaced at 12 inches [305 mm] on center spanning in the horizontal direction. The nominal steel yield strength was 60,000 psi [414 MPa]. The slab was supported at the top and bottom only to achieve vertical one-way flexural behavior, consistent with the primary reinforcing being in the vertical direction. Details of the supports are shown in Figure 1.

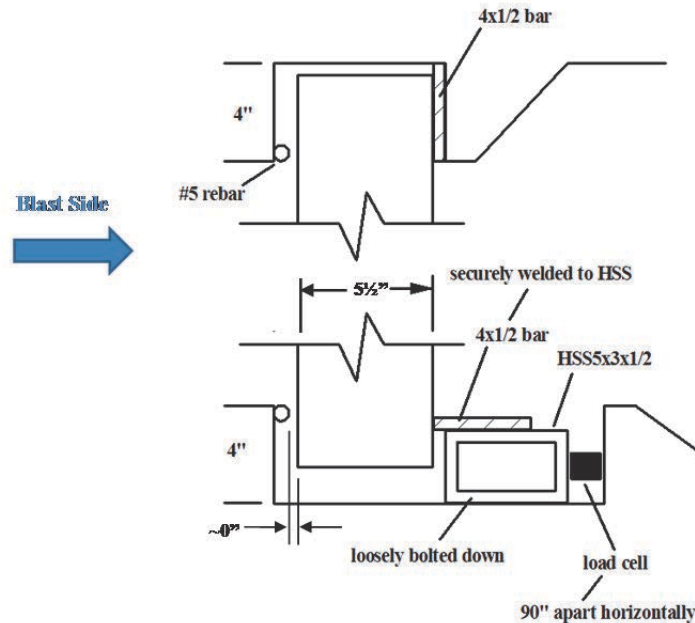


Figure 1 — Slab Support Conditions for Shock Tube Tests

The blast tests were conducted at the BakerRisk’s large shock tube facility (Figure 2). The shock tube consists of two major sections, a driver section and an expansion section. Blast pressures are generated when a rupture diaphragm placed between the two sections fails at a specified pressure in the driver section. A shock wave then propagates along the expansion section and loads the test specimen at the end of this expansion section.



Figure 2 — BakerRisk Large Shock Tube

Within the series, two tests (numbered 1 and 6) were conducted on baseline slabs with no rebar couplers. These tests were chosen for use in this analytical study, since they eliminate the potential complications introduced by the use of mechanical couplers. The tests were conducted at different levels of loading, with test 1 registering a peak applied pressure of 7.7 psi [53 kPa] while test 6 reached 10.6 psi [73 kPa]. The impulse in test 6 was also significantly higher. The applied pressure, as measured from three pressure gauges mounted in the shock tube wall only 3 inches [76 mm] upstream from the face of the wall, is presented in Figure 3. The curve shown for each test represents the average of the three gauges (the variability among the individual gauges was relatively small). Aside from the change in loading, the two experiments were otherwise identical.

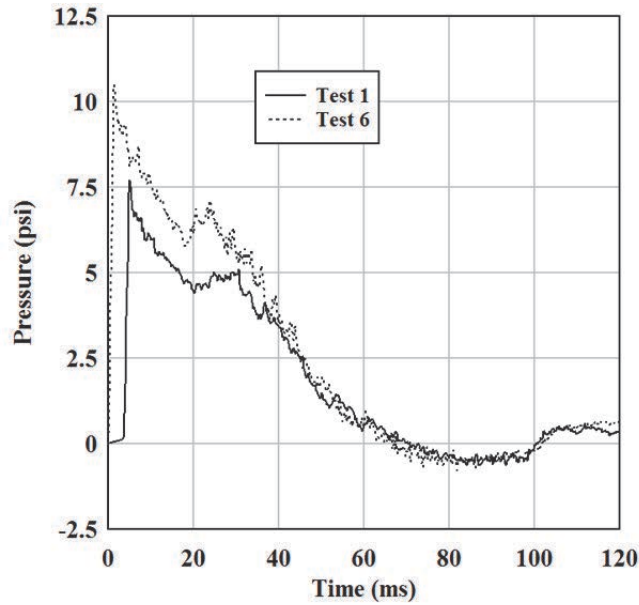


Figure 3 — Blast Wave Profiles from Shock Tube Tests 1 and 6

In addition to the pressure gauges, high speed cameras recorded the response of the slabs when subjected to the blast loads. By recording the position of the slab back face at various times over the duration of the video record, a displacement history of the slab centerline was obtained for each test, as plotted in Figure 4. As the figure indicates, the response in test 6 is nearly three times as large as that in test 1, even though the applied load was only incrementally larger. We also observe that the slab in test 1 experienced significant rebound even though the deflection went well into the plastic regime, with the late-time displacement being under half an inch [12 mm] (20% of peak), whereas test 6 produced a late-time residual displacement of approximately 2 inches [51 mm] (30% of peak). A possible factor here may be the presence of late-time negative phase loads produced by the shock tube.

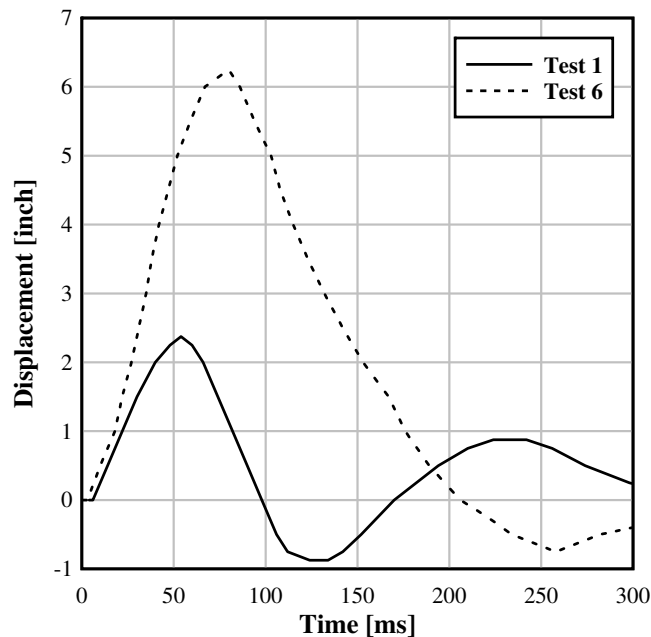


Figure 4 — Slab Centerline Displacement Histories

For convenience, Table 1 contains a summary of the key blast metrics and results from the two tests. Note that the peak support rotation (which is the typical way of characterizing damage) is around 3 degrees in test 1, while the test 6 result is around 7 degrees. Typical damage criteria for reinforced concrete slabs without shear reinforcing indicate a transition from medium to high damage at 2 degrees, and from high damage to failure at 5 degrees^[2]. Using these criteria, the test 1 slab would be labeled “high damage” while the test 6 slab would be at “failure.” Figure 5 shows photos of the slabs after each test, viewed from the downstream side of the slab (i.e., the non-loaded side). The slabs clearly responded in vertical one-way action, with consistent horizontal cracks across their entire width. The degree of cracking visible in test 1 is quite minor, and even though there is some small residual displacement, labeling this result as “high damage” is clearly conservative. Furthermore, while the test 6 slab shows some large visible cracks and significant permanent deformation, it appears to be in no danger of imminent failure. These observations reinforce the heavily conservative approach typically used to define damage criteria for design purposes.

Table 1 — Key Metrics from Slab Tests

Test No.	Applied Pressure (psi) [kPa]	Applied Impulse (psi·ms) [kPa·ms]	Peak Deflection (in) [mm]	Peak Support Rotation (°)
1	7.7 [53]	217 [1,500]	2.4 [61]	2.7
6	10.6 [73]	297 [2,050]	6.2 [157]	7.1



Test 1

Test 6

Figure 5 — Post Test Photos of Slab Surface (Non-Loaded Side).

Actual concrete strengths for the test articles were not experimentally obtained. The concrete mix was specified as having a nominal 28-day compressive strength of 4,000 psi [27.6 MPa]. The two slabs had somewhat different cure time at their respective test dates. A reasonable estimate of the test-day strength of the concrete is 3,900 psi [26.9 MPa] for Test 1 and 4,400 psi [30.3 MPa] for Test 6, using standard curves for concrete aging and assuming a 28-day static increase factor of 1.1 over the nominal design strength of the concrete mix.

FINITE ELEMENT MODEL

A 3D finite element model was defined to represent the test slab and its supports. For consistency, a single mesh was used in the analyses using all three material models. The model is shown schematically in Figure 6, rotated 90° for convenience. Hexahedral (solid brick) elements were used to represent the concrete, with six elements through the slab's thickness. As a result, the concrete element size is slightly less than 1 inch in each dimension (0.96×0.96×0.92 inch, to be precise).

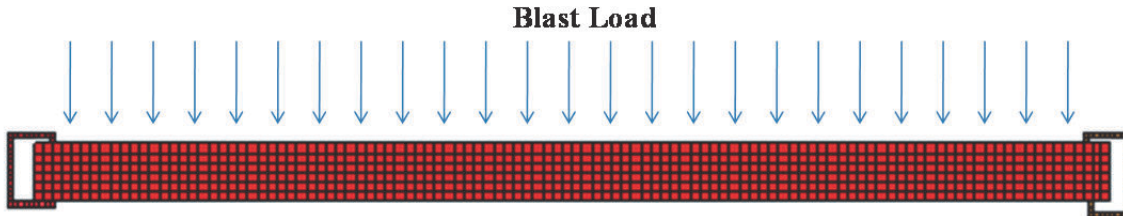


Figure 6 — Section View Through the Concrete Slab (Shown Rotated 90°)

A mesh convergence study would have been of additional interest, but may also have distracted attention from the primary purpose of this study, as each constitutive model may have reached a target convergence tolerance at varying levels of mesh refinement. Instead, since our goal was to exercise all models using the same mesh, a fixed mesh size was used for all three models. Experience with calculation of blast-loaded slabs has indicated that a mesh with six elements through the thickness is a reasonable lower bound for practical problems. More elements are certainly better, but for typical applications, this level of mesh refinement has historically produced satisfactory results.

Beam elements were used to represent the reinforcing. Both vertical and horizontal rebar were collocated at the mid-plane of the slab, using shared nodes between the beams and the solid elements (no provision for bond-slip between rebar and concrete). For a slab response in the light to moderate range of damage, inclusion of bond-slip is not typically required since the amount of slippage is negligible. The steel supports were modeled with an elastic material that was rigidly supported, with contact defined between the slab and the steel. The boundaries replicate the actual conditions in the test article, and are similar to simply-supported conditions. Note that the slab is unable to develop any arching or membrane behavior.

Because of the symmetry of the slab, a vertical half-segment was included in the model with a symmetry boundary applied along the vertical centerline. The blast load measured in each test (Figure 3) was applied as a uniform dynamic pressure over the entire slab surface.

The reinforcing steel used in the test articles was ASTM A 605 Grade 60 rebar, with a minimum yield strength of 60 ksi [414 MPa]. The steel was represented in the finite element model using an elastic-plastic model (MAT3 in the LS-DYNA and DYNA3D material libraries). For those runs which involved rate sensitivity in the concrete (see discussion below), the steel strength was increased from its nominal 60 ksi [414 MPa] with a static increase factor of 1.1 (to represent realistic vs. minimum strength) and a dynamic increase factor of 1.22. A tangent modulus of 230 ksi [1,590 MPa] was included to represent post-yield hardening behavior. Failure was not included in the steel model as the rebar did not reach significantly high strains, nor was failure observed in either of the experiments themselves.

CONCRETE MATERIAL MODELS

Three different concrete models were evaluated in this study; the primary features of each are briefly summarized below. The models were chosen since they are implemented within widely available explicit finite elements codes, are broadly used within the blast effects community, and are familiar to the authors.

AEC-3I model

The Applied Engineering Cap Model with Three Invariants (AEC-3I)^[3] was implemented into DYNA-3D under a license/collaboration agreement with Lawrence Livermore National Laboratory. The AEC-3I models material plasticity with a unified shear yield and cap surface that can harden from an initial yield position to ultimate strength, and then soften to residual surfaces under continued loading. The cap portion of the yield surface only hardens and does not soften. The AEC-3I incorporates standard predictions of elastic stresses until a yield surface is reached. The AEC-3I uses a non-associated flow rule in the form of normal stress correction to the yield surfaces. Dilation and shear compaction are controlled through relative strain hardening parameters of the shear yield surface and cap, respectively. The shear yield surface provides strength dependence upon mean normal stress, which typically represents the behavior of frictional materials such as concrete, rock, ceramics and soils. The yield surfaces are also a function of the intermediate principal stresses (third invariant) for modeling strength dependence on stress state (triaxial compression, extension, and torsion). Strain softening is dependent on mean normal stress for modeling brittle compressive failure at low pressures, transitioning to ductile behavior at high pressures.

A decohesion model for modeling tensile fracture and crack growth^[4] was married with the plasticity of the AEC-3I model in a program funded by the Defense Threat Reduction Agency (DTRA) in 2005 and 2006. The decohesion algorithms model the formation of crack planes with defined orientation, and controlled growth based on material fracture energy, specified as a user input. Crack growth is represented with decohesion strain components resulting in anisotropic material behavior. Finite elements cannot carry traction forces across a fully formed crack plane, and subsequent compressive forces are not engaged until the crack has closed. Crack formation does not modify the shear yield surfaces of the material. Any number of crack failure planes can form and grow within any finite element. Orientation of crack plane initiation is based on principal-stress Rankine criteria, characteristic of brittle-fracture materials. Use of these criteria results in efficient computational speeds similar to standard plasticity models.

The AEC-3I/decohesion model does not incorporate strain rate effects on material properties. Instead, dynamic strength enhancement is modeled by explicit (offline) application of an increase factor to the compressive and tensile strength values.

MAT72R3

Material 72 in the LS-DYNA material library (identified as MAT_CONCRETE_DAMAGE_REL3) was the second model used to represent the concrete. This material model consists of three shear failure surfaces, the initial yield surface, the maximum yield surface and the residual yield surface.^[5, 6] During initial loading, the deviatoric stresses are elastic until the initial yield surface is reached. The stresses can then increase further until these reach the maximum yield surface. Beyond this stage, the response can soften to the residual surface or be perfectly plastic. Shear dilatancy, which occurs as concrete approaches failure,^[9] is incorporated in the model. The user has the option to take shear dilatancy into consideration via the fractional dilatancy parameter ω ; the parameter can range from 0.0 to 1.0, with a default value of 0.5. A softening model for concrete in tension is also included in the material model.

One noteworthy feature of the model is its ability to accept user input of two separate curves defining the dynamic increase factor as a function of strain rate, one curve for tension and another in compression. This allows the model to represent the significant differences that have been observed in physical experiments between rate enhancement in tension and compression.

MAT159

Material 159 from the LS-DYNA material library^[7] (identified as MAT_CSCM_CONCRETE) was also used to represent the concrete. This material model has a smooth intersection between the failure surface and the hardening cap and is often referred to as a Continuous Surface Cap Model (CSCM).^[7] The model parameters are fit to data for unconfined compression strengths between approximately 4,000 and 8,400 psi [27.6 and 57.9 MPa]. Shear dilatancy, which occurs as concrete in compression approaches failure,^[7, 9] is incorporated in the model. The

softening of concrete after the peak stresses have been reached is modeled via a damage formulation. This formulation models strain softening and modulus reduction for both tensile and compressive hydrostatic pressures. The concrete model also includes strain rate dependence for tensile and compressive states of stress, as well as for fracture energy. Default values of parameters controlling the rate sensitivity were used in these calculations.

CONCRETE MODEL FEATURES

Two model features, their representation of strain rate enhancement and their ability to represent stress states for material that is loaded cyclically, are discussed below.

Strain rate enhancement

The apparent enhancement of both compressive and tensile strength of concrete when loaded rapidly (i.e., at high rates of strain) has been well documented in numerous earlier studies. The three models considered in this paper treat concrete rate sensitivity in varying ways, as described above. In order to better evaluate the models on a consistent basis, the following finite element analyses were conducted.

First, as a baseline, the static concrete strength was used with no rate enhancement of any kind.

Second, a constant dynamic increase factor (DIF) was applied to the concrete strength as part of the input, without using actual rate-dependent features of the material models. In this study, a DIF of 1.19 was applied to the static compressive strength; since the tensile strength is computed internally by all three models using a square-root formulation, the effective DIF in tension would be 1.10. The value of 1.19 was obtained from guidance contained in standard published design manuals^[10] for reinforced concrete sections in bending.

Third, fully rate-dependent properties were used in models MAT72R3 and MAT159 only; the AEC-3I model does not have strain rate dependence as an option. In the case of MAT159, the rate dependence (DIF as a function of strain rate) is internally fixed via a hard-wired function with no user inputs. In the case of MAT72R3, the user is able to input DIF curves in both tension and compression. The curves used in this study were computed as a function of the static compressive strength using the approach derived by Malvar,^[11] which in turn is based on the recommendations of the European concrete design code.^[12]

Figure 7 plots the rate curves used by these two models in tension and compression along with the constant DIF values. Note the dissimilar vertical scales in the two plots: the rate enhancement in tension greatly exceeds that in compression as the rate goes beyond 1 s^{-1} . We also see that the constant DIF value is quite conservative for all but the very lowest strain rates, as would be expected in a design context.

Cyclic loading

One potentially important feature of a concrete constitutive model is its ability to represent the material's behavior when undergoing cyclic loading. In particular, if the concrete is first loaded in tension, cracks and fails, and then is reloaded in compression, the material's ability to model the crack formation followed by closing of the crack and eventual reloading in compression would be very relevant to its ability to represent slab response, particularly in the time domain following peak response and during the rebound phase.

To evaluate our three models, a simple single-element calculation was performed in which a 1-inch cube of concrete was subjected to a displacement constraint on one surface while being held on the other. The cube was allowed to expand or contract laterally (unconfined condition with uniaxial vertical stress). The applied displacement history can thus be converted to a vertical strain, as plotted in Figure 8. The element is first elongated to a tensile strain of 1%, after which the strain is reversed and the element is shortened back to its original length and beyond.

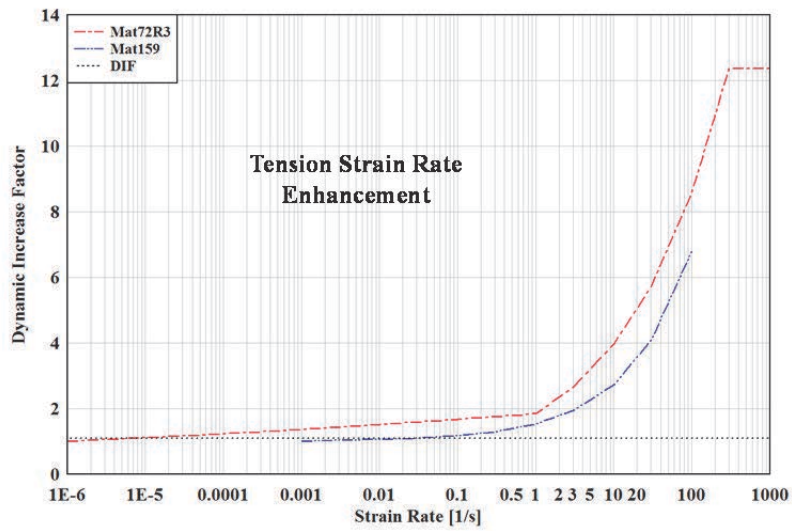
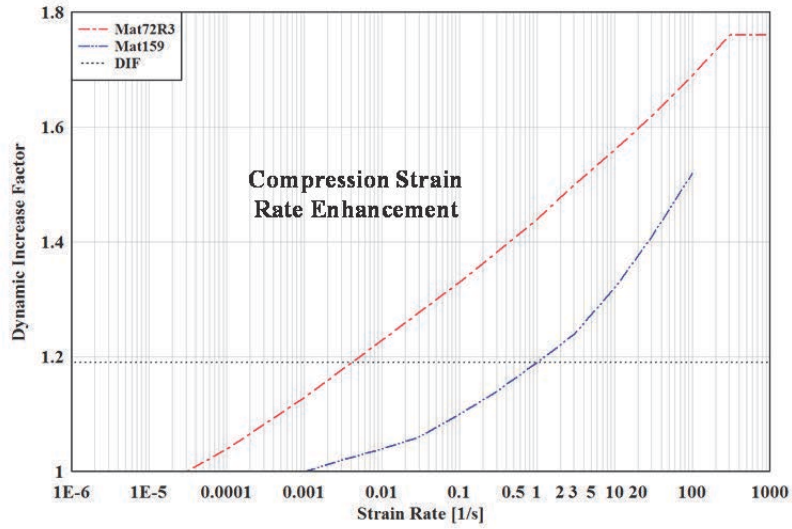


Figure 7 — Concrete Strain Rate Enhancement Curves Compared to DIF

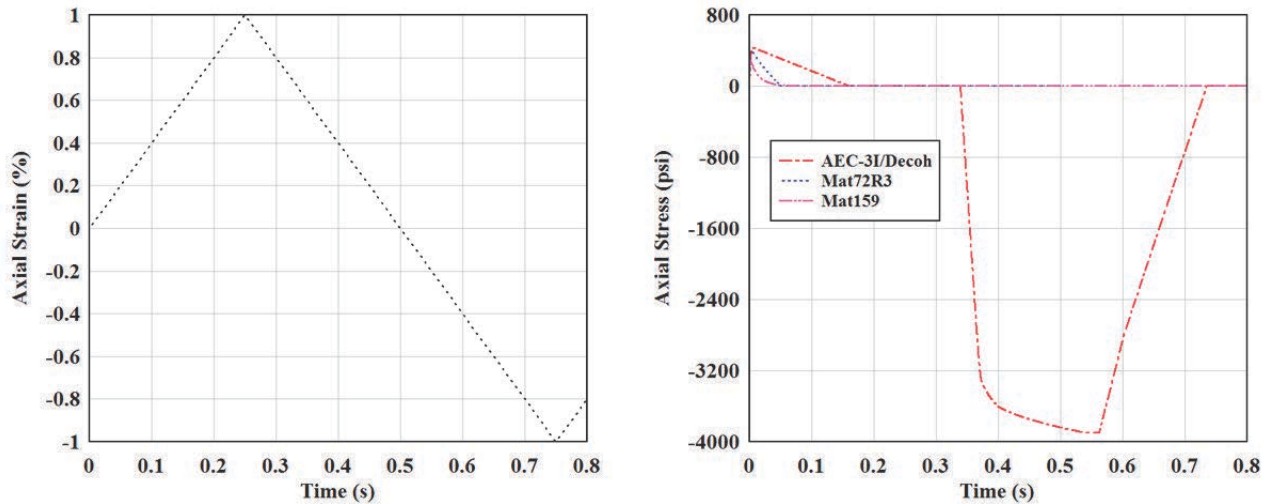


Figure 8 — Axial Strain and Stress from Single-Element Cyclic Loading Test